Journal of Materials Chemistry

Cite this: J. Mater. Chem., 2012, 22, 4759

www.rsc.org/materials

PAPER

Solvothermal synthesis of electroactive lithium iron tavorites and structure of Li_2FePO_4F

B. L. Ellis,[a] T. N. Ramesh,[a] W. N. Rowan-Weetaluktuk,[b] D. H. Ryan[b] and L. F. Nazar*[a]

Received 17th October 2011, Accepted 20th December 2011
DOI: 10.1039/c2jm15273h

Lithium transition metal fluorophosphates with a tavorite structure have been recognized as promising electrode materials for lithium-ion batteries because of their good energy storage capacity combined with electrochemical and thermal stability. We report here a new low-cost and environmentally friendly solvothermal process to prepare $LiFePO_4F$, which exhibits a complex single phase regime followed by a two-phase plateau at 2.75 V on electrochemical lithium insertion. The structure of the pure single phase end member Li_2FePO_4F was synthesized by lithiation of $LiFePO_4F$, and solved *via* Rietveld refinement of the combined X-ray and neutron diffraction patterns, showing that Li^+ occupies multiple sites in the tavorite lattice. $LiFePO_4OH$ was prepared by a new synthetic route and the electrochemical capacity for this material is the highest reported to date. $LiFePO_4OH$ was found to intercalate lithium at 2.40 V and the reduced Li_2FePO_4OH phase was found to be amorphous.

Introduction

Transition metal polyanionic compounds such as phosphates, fluorophosphates and fluorosulfates are considered promising positive electrode materials for lithium-ion batteries. These members of the lithium metal polyanion family have been a major focus of research for reasons of high safety, low cost and low environmental impact.[1] The most prominent compound of this group studied to date has been olivine $LiFePO_4$.[1,2] The major limitations of $LiFePO_4$, namely poor electrical conductivity and one-dimensional Li-ion diffusion,[3] have been largely overcome by decreasing the crystallite size to the nano-scale[4] and by coating conductive additives onto the surface.[5,6] However, these approaches add to the complexity and reduce the reliability of the material's manufacture. Other promising positive electrode materials in polyanion family include fluorophosphates that do not present this 1-D ion conductivity challenge include Na_2FePO_4F,[7,8] $LiFePO_4F$,[9,10] $LiVPO_4F$[11,12] and a new category of fluorosulphates such as $LiFeSO_4F$.[13,14] All but the first crystallize in the tavorite family - $LiMPO_4(OH)_xF_{1-x}$ (M = V, Fe, Al) - which present exciting possibilities from an ion transport point of view. These compounds are comprised of one-dimensional chains of metal octahedra interconnected by polyanion tetrahedra which allow 1-D electron transport, while intersecting channels that house the Li^+ afford open pathways for 3-D ion transport. Several compounds with this structure demonstrate high ionic conductivity at high temperatures, including the mineral tavorite, $LiFePO_4(OH)$[15,16] and $LiMgSO_4F$.[17]

Many phosphate and fluorosulfate compounds have been synthesized previously by hydrothermal or solvothermal routes where water or an inexpensive organic compound was used as the solvent, including the olivines $LiFePO_4$[18,19] and $LiMnPO_4$,[19] layered Na_2FePO_4F,[7] and the tavorites $LiVPO_4F$,[20] $LiFePO_4(OH)$[15,21] and $LiMSO_4F$ (M = Fe, Mn, Co, Ni).[13,22] Hydrothermal and solvothermal synthetic routes offer significant advantages compared to conventional solid-state techniques in terms of reaction time and energy consumption. These reaction techniques are also industrially viable, as hydrothermal syntheses are readily scalable to produce large quantities of material and the reaction media is inexpensive (water or an low cost organic solvent). In the case of the fluorosulphates, the solvents used for solvothermal synthesis include inexpensive glycols[13] or costly ionic liquids[14,22] – the latter which must be recaptured and recycled. $LiFePO_4F$ has also been synthesized in cost-prohibitive ionic liquid media.[10]

Two fluorophosphates of the tavorite family, $LiFePO_4F$ and $LiVPO_4F$, have previously been explored as positive electrode materials. The $V^{3+} \rightarrow V^{4+}$ transition in $LiVPO_4F$ is located at 4.25 V *vs.* Li/Li^+.[11] $LiVPO_4F$ has also been shown to intercalate Li: the $V^{3+} \rightarrow V^{2+}$ transition is at 1.75 V *vs.* Li/Li^+, a potential low enough to demonstrate cycling of a symmetrical cell based on $LiVPO_4F$.[23] In $LiFePO_4F$, $Fe^{3+} \rightarrow Fe^{2+}$ redox couple is at 2.8 V *vs.* Li/Li^+,[9] about 0.7 V lower than the same redox transition in $LiFePO_4$, owing to a reduced influence of the inductive effect. The phosphate groups in olivine share edges with the metal octahedra whereas in the tavorite structure, the corner-sharing reduces the repulsion between metal centres and hence lowers the

[a]University of Waterloo, Department of Chemistry, 200 University Ave. W., Waterloo, Ontario, Canada N2L 3G1. E-mail: lfnazar@uwaterloo.ca
[b]Department of Physics, McGill University, Canada H3A 2T8

potential. Each of the electrochemical transitions reported in the tavorite fluorophosphates reported previously exhibit primarily two-phase behavior on both lithium intercalation and deintercalation, due to strong ion-electron interactions.

Here, we report a new solvothermal synthesis of nanocrystalline iron tavorite $LiFePO_4F$ using ethanol as the solvent, and report its thermal stability compared to the hydroxy-tavorite, $LiFePO_4OH$. We explore the nature of its complex single and two phase electrochemical behavior *via* measurements combined with *ex-situ* X-ray diffraction studies. Moreover, we report the first structural solution of the electrochemical end member, Li_2FePO_4F, based on a combined refinement of X-ray and neutron diffraction data. This follows on our previous iron tavorite report where only the lattice parameters of this phase were obtained by a LeBail fit of X-ray diffraction data.[9] The structure is revealed to be surprisingly complex; Mössbauer spectroscopy was used to elucidate the structural subtleties and to verify the full reduction of Fe^{3+} to Fe^{2+} in Li_2FePO_4F. Furthermore, chemical reduction of $LiFePO_4OH$ to Li_2FePO_4OH revealed a transition to an amorphous phase, which explained the change in electrochemical potential observed after the first discharge cycle of $LiFePO_4OH$.

Experimental

$LiFePO_4OH$

In a typical synthesis, 1.78 g of an iron phosphate precursor ($FePO_4 \cdot 1.5H_2O$, prepared as previously reported[24]), was combined with 0.25 g $LiOH \cdot H_2O$ and 0.10 g lithium acetate ($Li(CH_3COO) \cdot 2H_2O$) and 10 ml of deionized water in a 23 ml Teflon lined Parr acid digestion bomb. The mixture was stirred for 30 min and heated to 160–200 °C for 8–15 h. The yellow product was filtered, washed with deionized water and dried under vacuum at 80 °C for 16 h.

$LiFePO_4F$

1.13 g of anhydrous FeF_3 and 1.04 g of LiH_2PO_4 were stirred in 15 ml of ethyl alcohol in a 23 ml Teflon lined Parr reactor. The mixture was heated to 230 °C for 3 days. The light grey product was filtered, washed with deionized water and dried under vacuum at 80 °C for 16 h. A solid-state method was also used to prepare $LiFePO_4F$, as previously outlined.[9]

$Li_{1+x}FePO_4(F,OH)$

To intercalate Li into $LiFePO_4F$, material prepared by the solid-state method was stirred with stoichiometric amounts of $LiAlH_4$ for 44 h in tetrahydrofuran in an argon filled glove box and filtered to produce single phase Li_2FePO_4F. $LiFePO_4OH$ was reduced with stoichiometric amounts of n-butyl lithium.

Materials characterization

Powder X-ray diffraction was performed on a Bruker D8-Advance powder diffractometer using Cu-Kα radiation (λ = 1.5405 Å), operating from $2\Theta = 10°$ to 80° at a step size of 0.01° with a count time of 5 s per step. Neutron diffraction data was collected on a 3 g sample of Li_2FePO_4F using the HB2A High Resolution Powder Diffractometer at the High Flux Isotope Reactor at the Oak Ridge National Labs (Tennessee, USA). Samples of $Li_{1+x}FePO_4F$ were loaded in a hermetically sealed holder to prevent air exposure. Lattice parameters were initially determined using TOPAS™ software and structural refinements were carried out with the GSAS program[25] with the EXPGUI interface[26] using full pattern matching. Scale factor, zero point, background, lattice parameters, atomic positions and thermal factors were iteratively refined.

Powder samples for SEM were gold coated and examined in a LEO 1530 field emission scanning electron microscope (FESEM) equipped with an energy dispersive X-ray spectroscopy (EDX) attachment. Images were recorded at 15 kV with a back-scattered electron detector. For thermal gravimetric measurements, 10–20 mg samples were placed in an alumina crucible and heated at 10 °C min^{-1} under air (100 mL min^{-1}) using a SDT Q-600 TGA from TA Instruments. A Bruker Tensor infrared spectrometer was used to collect spectra of as-prepared materials ground with KBr and pressed into pellets. Elemental analysis of Li_2FePO_4F was performed by inductively coupled plasma mass spectrometry.

Mössbauer spectra were collected over a counting time of 20 h in a hermetically sealed holder using a 50mCi $^{57}CoRh$ source mounted on a constant-acceleration spectrometer calibrated using α-Fe foil at room temperature. Fitting was accomplished using standard least-squares methods.

For electrochemical measurements, materials were mixed with carbon black and polyvinylidene difluoride in a 75 : 15 : 10 weight ratio. The cell loading was 5–6 mg cm^{-2}. The electrochemical measurements were conducted in 2220 coin cells, using a lithium metal anode and an electrolyte solution comprised of 1M $LiPF_6$ in 1 : 1 ethylene carbonate/dimethyl carbonate. Room temperature galvanostatic cycling was performed between 1.5 and 4.0 V.

Discussion

$LiFePO_4F$ prepared by solid state methods where the sample is heated under flowing argon produces a pure single phase material as we have previously reported,[9] in contrast to previous studies where the sintering environment was air.[12] The solvothermal technique reported here also produces single phase $LiFePO_4F$ - at a much lower temperature than the solid state or other solution-based methods - and without the need to recover expensive ionic liquids.[10] Precautions are necessary, however. The precursors were dried in an oven at 100 °C and the ethanol was dried over molecular sieves prior to starting the reaction to minimize water and suppress OH^- formation in solution. X-ray diffraction patterns, indexed in $P\bar{1}$, and FESEM images of $LiFePO_4F$ that compare the products from the solid state and solvothermal methods are shown in Fig. 1a and b. Reagent choice and pH control in the latter is critical in order to ensure $LiFePO_4F$ is the only product. For example, the addition of NH_4HF_2 which acts as both a fluorinating agent and a weak acid favored the formation of giniite, $Fe_5(PO_4)_4(OH)_3 \cdot 2H_2O$, which precipitates in acidic media.[27] The solid-state prepared material forms agglomerates of large (300–1000 nm) particles typical of carbon-free high-temperature synthesis routes. Conversely, the solvothermally produced $LiFePO_4F$ has a matchstick-like morphology: crystallites exhibit very small dimensions

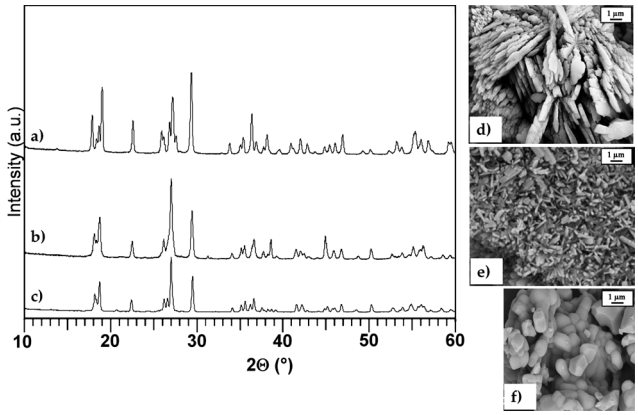

Fig. 1 (a–c) X-ray diffraction patterns and (d–f) corresponding SEM images of $LiFePO_4(OH)$ (a,d), $LiFePO_4F$ prepared by the solvothermal route (b,e) and $LiFePO_4F$ prepared by a solid-state route (c,f).

(<100 nm) in two directions with lengths up to 1 μm. The lattice parameters for materials prepared by both methods are given in Table 1.

The triclinic ($P\bar{1}$) structure of $LiFePO_4F$ has been previously reported;[9] a polyhedral representation of the structure is shown in Fig. 2a. $LiFePO_4F$ is comprised of one-dimensional chains of corner-sharing $[FeO_4F_2]$ octahedra - which effectively limit electron transport to one dimension - connected by corner-sharing phosphate tetrahedra. The resulting cavities house the Li^+ and afford open pathways for 3-D ion transport. Several compounds with this structure demonstrate high ionic conductivity including $LiFePO_4(OH)$.[15,16] $LiFePO_4(OH)$. is isostructural with $LiFePO_4F$, except the hydroxide ions act as bridging ligands instead of F^-. Replacement of F^- with OH^- results in subtle changes to the structure owing to its slightly larger size. A slight contraction in the *c* lattice parameter and an increase in the other lattice parameters was observed, leading to a small increase in the overall unit cell volume from 173.6 $Å^3$ for $LiFePO_4F$ to 174.8 $Å^3$ for $LiFePO_4(OH)$.

The hydrothermal method of preparation of $LiFePO_4OH$ yields micron-sized platelets of pure $LiFePO_4(OH)$, similar to the previously reported hydrothermal synthesis that utilizes similar temperature but slightly longer duration,[21] although reaction time is not a determining factor for particle morphology in the low-temperature hydrothermal preparation of phosphate materials.[19] This is much simpler and more efficient compared to a method that requires temperatures above 400 °C as well as excessive pressure and long periods of time to crystallize the material.[28] An X-ray powder diffraction pattern and a representative scanning electron microscope (SEM) image of the resultant material are shown in Fig. 1c. The indexed lattice parameters given in Table 1 are in accord with those reported for single crystal and polycrystalline samples of $LiFePO_4(OH)$.[21,28]

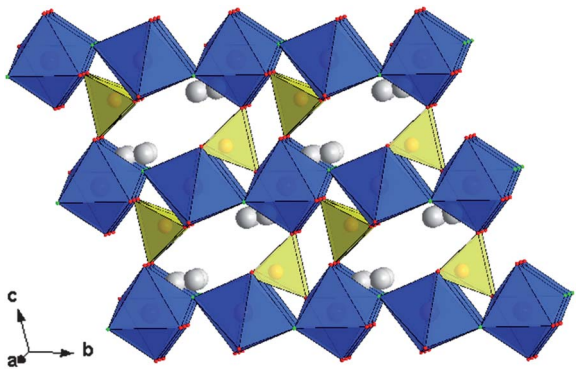

Fig. 2 Graphical representation of the $LiFePO_4F$ structure with iron octahedra in blue, phosphate tetrahedra in yellow and lithium ions in white.

Infrared spectroscopy was used to verify the presence of hydroxide moieties in $LiFePO_4(OH)$, and their absence in $LiFePO_4F$. The spectra are shown in Fig. 3. In the case of $LiFePO_4(OH)$, the ν(O–H) stretch is evident as a very strong peak at 3280 cm^{-1}, and a strong peak at 790 cm^{-1} corresponds to an O–H bending mode. For $LiFePO_4F$, there are no peaks in the 3000–3600 cm^{-1} or 750–800 cm^{-1} regions of the IR spectrum indicating that the compound is free of hydroxide and is thus fully fluorinated.

The thermal stability of each compound in air was determined using thermal gravimetric analysis and the results are shown in Fig. 4. $LiFePO_4F$ remains stable under ambient conditions up to 600 °C, at which point it reacts with moisture in the air according to the following reaction:

$$6\ LiFePO_4F + 3\ H_2O \rightarrow 2\ Li_3Fe_2(PO_4)_3 + Fe_2O_3 + 6\ HF$$

A mass loss of 6.0% was measured for this process, in excellent agreement with the calculated value of 6.2%. Not surprisingly,

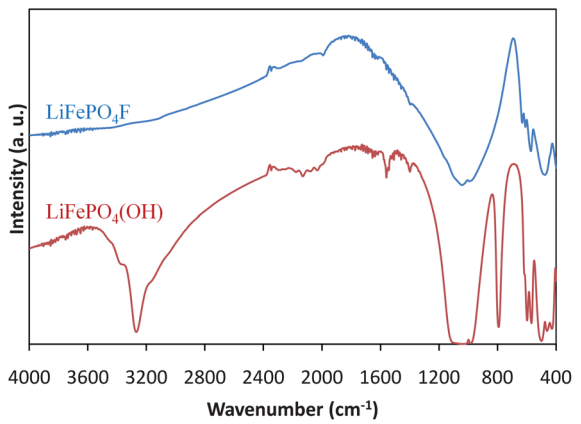

Fig. 3 Infrared spectra of as-prepared $LiFePO_4F$, and $LiFePO_4(OH)$.

Table 1 Lattice parameters of synthesized $LiFePO_4(OH)/F$

Compound	*a*/Å	*b*/Å	*c*/Å	α (°)	β (°)	γ (°)	*V*/$Å^3$
$LiFePO_4(OH)$	5.352	7.285	5.116	109.28	97.82	106.33	174.83
SS-$LiFePO_4F$	5.300	7.260	5.151	107.88	98.56	107.34	173.67
ST-$LiFePO_4F$	5.301	7.262	5.153	107.95	98.62	107.41	173.58

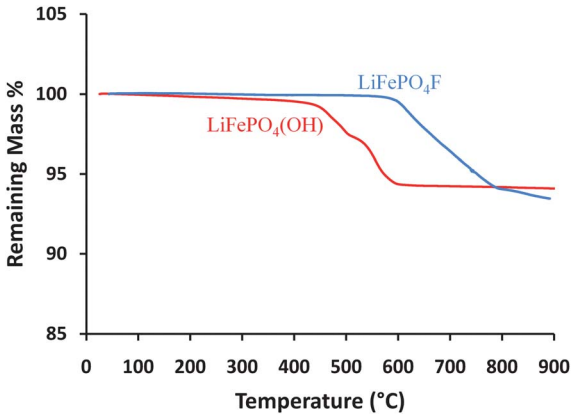

Fig. 4 TGA curves of $LiFePO_4F$, and $LiFePO_4(OH)$.

the solid materials produced from this reaction were also formed on thermal decomposition of olivine $LiFePO_4$ under oxidizing conditions.[29] $LiFePO_4F$ is more stable in air than FeF_3, which was found to hydrolyze at 450 °C.[30] $LiFePO_4(OH)$ decomposes near 450 °C, close to that reported for the decomposition of $LiFePO_4(OH)$ under pure oxygen,[29] and at a significantly lower temperature than that we observed for $LiFePO_4F$. X-ray diffraction identified both $Li_3Fe_2(PO_4)_3$ and Fe_2O_3 as decomposition products of $LiFePO_4(OH)$. Clearly, the presence of fluoride in the tavorite crystal structure increases the thermal stability of these compounds.

Electrochemical profiles of as-prepared and pulverized samples of $LiFePO_4F$ cycled at a slow rate (C/50) are shown in Fig. 5. The initial discharge of the as-prepared sample features a short plateau at 2.75 V followed by a long sloping overcharge (Fig. 5a). Since the electrode is comprised of rather large particles of $LiFePO_4F$ which are not carbon-coated, the as-prepared material has a low capacity for Li intercalation (0.55 Li) as well as high polarization (0.25 V). These shortcomings are eradicated by pulverizing the as-synthesized material for 3 h in a planetary ball mill. Although even one hour of ball-milling was sufficient, more than 3 h was counterproductive. An SEM micrograph of the active material after milling is shown in the inset of Fig. 5b. The particle morphology has changed significantly from the as-prepared material (see Fig. 1). After milling, the particles have a spherical shape and range in size from 200–400 nm, and the carbon is better dispersed. For this material, the electrochemical profile exhibits a sloping curve up to the insertion of 0.4 Li into the structure, at which point the profile is flat. This plateau is also at 2.75 V *vs.* Li. The cell can reach full capacity (152 mAh/g) and the polarization of this cell is small (0.10 V). As we reported previously, little capacity fade on cycling was observed for this material.[9] The electrochemical profile of the solvothermally-prepared $LiFePO_4F$ is shown in Fig. 5c. Although the material already has a very small particle size, milling with carbon (20–30 min) was necessary to increase the conductivity of the electrode. The profile has longer sloping regions but it still has a plateau at 2.75 V for a small portion of the cycle. The capacity of this material is slightly lower as only 0.8 Li is intercalated on the first cycle although this may be due to insufficient dispersion of the conductive carbon black. Although grinding the carbon-free sample after preparation clearly reduces the primary particle size

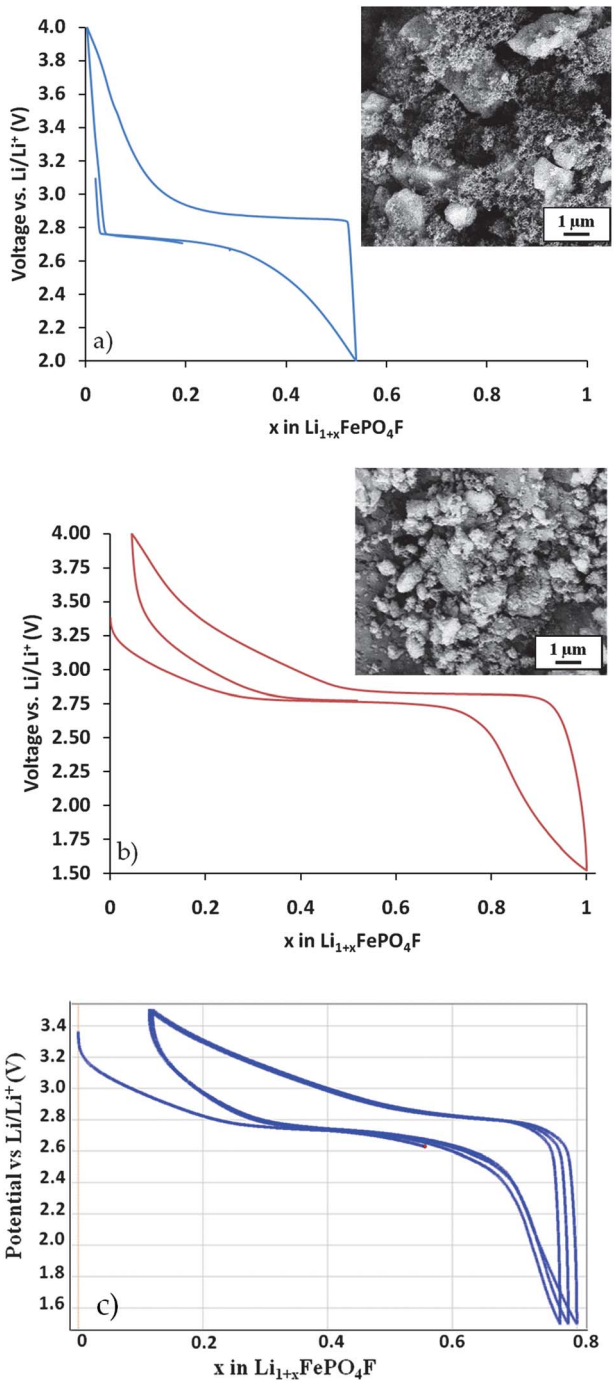

Fig. 5 Electrochemical data for $LiFePO_4F$ *vs.* Li/Li^+ collected in coin cells at a rate of C/50 for a) as-synthesized solid-state $LiFePO_4F$; b) solid-state $LiFePO_4F$ ground in a ball mill for 3 h; solvothermal $LiFePO_4F$ ball-milled for 30 min. SEM images of prepared electrodes for each material are shown in the inset.

of the electrode material, it is unclear whether the increase in electrode performance and change in profile shape are strictly the result of particle size reduction or whether other factors, such as the change in particle shape or formation of an amorphous iron fluorophosphate phase, are responsible. However, regardless of the method of sample preparation, $LiFePO_4F$ exhibited a flat voltage plateau at 2.75 V, indicative of a two-phase transition.

Electrochemical results for Li-ion cells based on the other anion composition, $LiFePO_4(OH)$, are presented in Fig. 6. The theoretical gravimetric capacity for insertion of 1 Li into $LiFePO_4(OH)$ is 154 mAh/g, slightly higher than that of $LiFePO_4F$. As with $LiFePO_4F$, the $LiFePO_4(OH)$ cells were prepared by ball-milling the as-prepared material for various lengths of time. The first discharge profiles of cells comprised of as-synthesized $LiFePO_4(OH)$, as well as material milled for 1–3 h are shown in Fig. 6a. Each $LiFePO_4(OH)$ cell has a flat plateau. However, the voltage of the as-prepared sample (2.30 V) is significantly lower than that of the sample milled for 1 h or milled for 3 h. This subtle increase in potential as a result of particle size reduction has also been reported for the olivine $LiFePO_4$ system.[31,32] The discharge capacity is also improved by decreasing the $LiFePO_4(OH)$ particle size. Full cycle profiles and SEM micrographs of the electrode material for the as-prepared and the 1 h milled samples prior to cycling are shown in Fig. 6b,c. By decreasing the particle size of the as-synthesized material and effectively dispersing the conductive carbon after milling for 1 h, the discharge capacity increased from 0.7 to 0.95 Li, both capacities being greater than those reported recently.[21] Initial cycling of $LiFePO_4OH$ shows 5% capacity loss over the first ten cycles, although the electrochemical test conditions have not yet been optimized. Sharp capacity fade was observed for the sample ball-milled for 3 h. We note that subsequent discharge cycles for cells comprised of either as-prepared material or material milled for 1 h exhibit a plateau at 2.42 V *vs.* Li. The potential of $LiFePO_4(OH)$ is roughly 0.35 V less than that of $LiFePO_4F$, the result of the weaker electronegativity of the OH^- ion which decreases the influence of the inductive effect.[2]

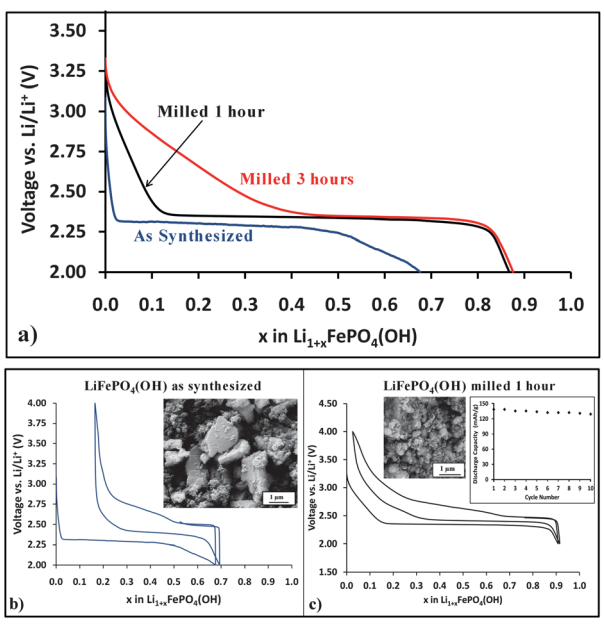

Fig. 6 Electrochemical data for $LiFePO_4(OH)$ *vs.* Li/Li^+ (rate of C/50). a) Initial discharge curves for as-synthesized hydrothermal $LiFePO_4(OH)$ (blue), $LiFePO_4(OH)$ ground in a ball mill for 1 h (black) and $LiFePO_4(OH)$ ground in a ball mill for 3 h (red). The first two full cycles for cells of the as-prepared and 1 h milled samples are shown in b) and c) respectively, with SEM images of the materials shown in the insets. Initial cycling for the 1 h sample is also shown inset in c).

The origin of this increase in discharge voltage of 0.12 V, seen on the second cycle (see above) was examined by chemical lithiation of $LiFePO_4(OH)$ to produce $Li_2FePO_4(OH)$, as outlined in Fig. 7. The $Li_2FePO_4(OH)$ material was black in colour. Powder X-ray diffraction, performed in an air-sensitive holder sealed under argon, revealed no crystalline diffraction peaks, as shown in Fig. 7b. The amorphous $Li_2FePO_4(OH)$ was chemically oxidized with NO_2BF_4 in an attempt to regenerate $LiFePO_4(OH)$. Again, an X-ray diffraction pattern was collected in a sealed holder under argon, and the pattern (Fig. 7c) indicated the material remained amorphous on oxidation. Based on these results, the electrochemical profile of $LiFePO_4(OH)$ may be explained: upon initial discharge, crystalline $LiFePO_4(OH)$ undergoes a transformation to an amorphous phase. The first charge cycle intercalates lithium ions into the amorphous structure and the second (and subsequent) charge and discharge cycles involve the (de)intercalation of lithium from this amorphous phase. Other positive electrode materials have been found to also undergo structural rearrangements to amorphous phases on the first electrochemical cycle, most notably the high-capacity silicate Li_2MnSiO_4.[33] Upon exposure to air (Fig. 7d), the tavorite phase recrystallized, as the pattern of $LiFePO_4OH$ was clearly recovered.

To verify the two phase nature of the electrochemical reaction in $LiFePO_4F$, we prepared variable compositions of $Li_{1+x}FePO_4F$ ($0 < x < 1$) by chemical reduction of as-synthesized $LiFePO_4F$ with $LiAlH_4$. Powder XRD patterns of these compositions are shown in Fig. 8; for clarity, the region of 2Θ from 10–40 is highlighted and peaks of interest are indexed. On reduction to $Li_{1.25}FePO_4F$ ($x = 0.25$ Li) a new second phase is barely evident in the diffraction pattern, signaled by the appearance of a very weak reflection at $2\theta = 27.8°$. This peak becomes unambiguously evident at the composition $Li_{1.5}FePO_4F$. Subsequent reduction indicates continued growth of the new Li_2FePO_4F phase at the expense of $LiFePO_4F$ until complete intercalation of one equivalent of Li results, in accord with the electrochemical data. The stoichiometry of this phase was verified by elemental analysis which confirmed a Li:Fe:P

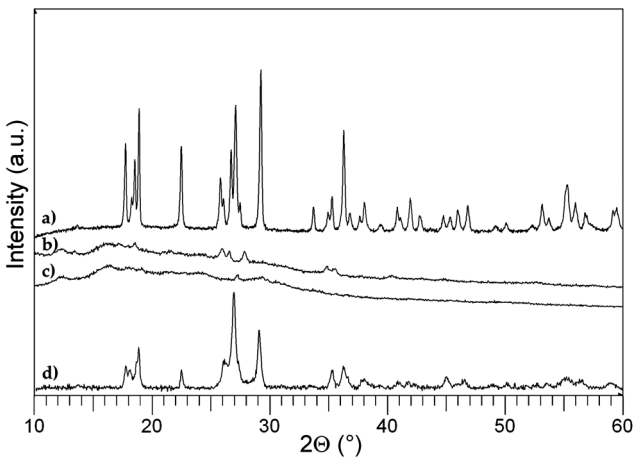

Fig. 7 X-ray diffraction patterns of a) as-prepared $LiFePO_4OH$; b) $LiFePO_4OH$ reduced with n-butyl lithium to make Li_2FePO_4OH; c) the chemical oxidation of Li_2FePO_4OH with NO_2BF_4 to make $LiFePO_4OH$; d) the material in c) exposed to air for 10 min at ambient conditions.

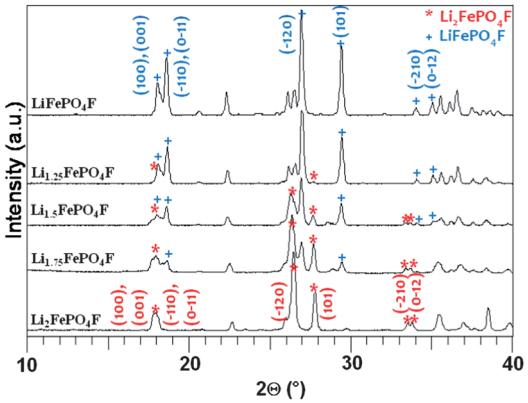

Fig. 8 XRD patterns of $Li_{1+x}FePO_4F$ compositions prepared by chemical reduction with stoichiometric amounts of $LiAlH_4$, showing the two-phase behavior upon $LiFePO_4F$ reduction. Selected peaks of $LiFePO_4F$ are shown with blue crosses and selected peaks of Li_2FePO_4F are shown with red asterisks.

ratio of approximately 2 : 1 : 1, and EDX measurements which confirmed a Fe:P:F ratio of very close to 1 : 1 : 1. In short, the existence of a solid solution between $0 < x < 0.3$ is unclear, but for $x > 0.4$, the existence of a two phase regime is unequivocal.

Mössbauer spectroscopy revealed very important clues about the lattice symmetry of $LiFePO_4F$, and especially Li_2FePO_4F. The Mössbauer spectrum for as-synthesized $LiFePO_4F$ is shown in Fig. 9a. The major signal (>90% of the total measured intensity) was fitted with a single isomer shift (IS) of 0.42(1) mm s^{-1} and quadrupole splitting (QS) of 1.15(1) mm s^{-1}, consistent with Fe^{3+} in the presence of an octahedral field. Although there are two crystallographically unique Fe^{3+} sites in $LiFePO_4F$, the two sites are very similar, with two fluoride and four oxygen ligands of similar bond lengths co-ordinated to both unique Fe atoms, and thus it is difficult to resolve the two sites. The Mössbauer spectrum and fit for the fully reduced material, Li_2FePO_4F are shown in Fig. 9b. Two distinct signals are clearly seen in the spectrum: the most prominent has parameters of IS = 1.24 mm s^{-1} and QS = 2.79 mm s^{-1} and the second signal has Mössbauer parameters of IS = 1.22 mm s^{-1} and QS = 2.18 mm s^{-1}. Together, these two signals make up about 90% of the total signal, which confirms the nearly full reduction of Fe^{3+} to Fe^{2+} in this sample. These two signals are in a (integrated) ratio of 2.9 : 1; ie close to 3 : 1. This is significant as $LiFePO_4F$ has only two unique Fe sites in the structure (Fig. 2). This unusual finding was also independently reported for a partially reduced sample without explanation.[10] It can be understood by structural effects.

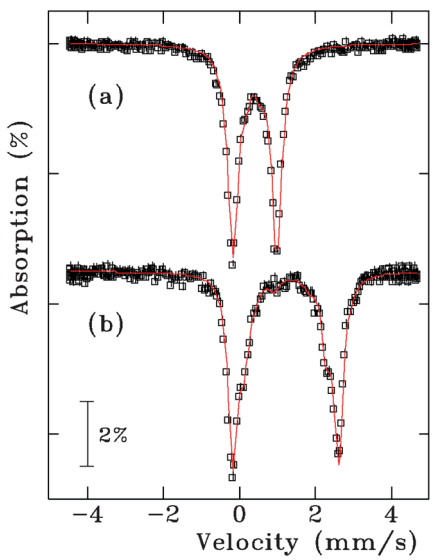

Fig. 9 Mössbauer spectra and fit (solid line) of a) $LiFePO_4F$ and b) Li_2FePO_4F, prepared from chemical reduction of $LiFePO_4F$ with $LiAlH_4$.

The structure of Li_2FePO_4F was elucidated by a combined Rietveld refinement of powder X-ray diffraction and neutron diffraction patterns. The fitted patterns are shown in Fig. 10a and b respectively and the refinement results are presented in Table 2. Indexing software indicated the space group for Li_2FePO_4F was $P\bar{1}$, the same as that of $LiFePO_4F$ which was used as the starting point for the refinement. The final refined lattice parameters are similar to those reported previously from a LeBail fit.[9] There is an 8.0% volume expansion of the $LiFePO_4F$ lattice upon Li intercalation. The iron fluorophosphate framework of Li_2FePO_4F is very similar to that in $LiFePO_4F$: 1-D chains of corner-shared FeO_4F_2 octahedra connected by PO_4^{3-} tetrahedra. Three

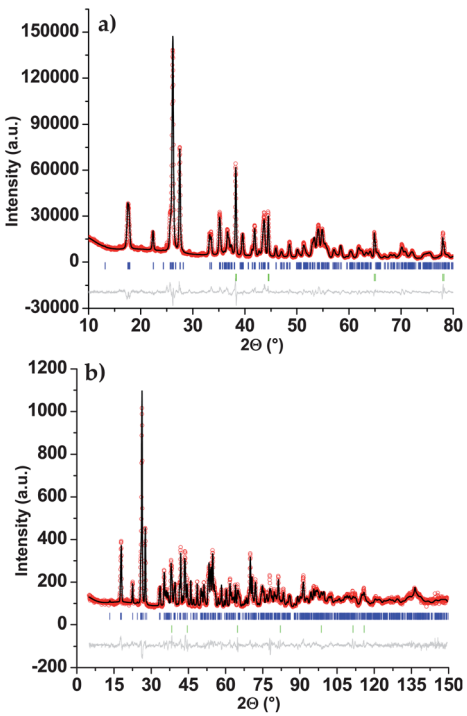

Fig. 10 Combined Rietveld refinement of X-ray and neutron powder diffraction data from a sample of Li_2FePO_4F. The statistical agreement factors for the combined refinement are: $R_{wp} = 9.45\%$, $R_p = 7.29\%$, $\chi^2 = 45.79$. a) Refined X-ray diffraction pattern with agreement factors of $R_{wp} = 9.48\%$, $R_p = 7.32\%$, $R_F^2 = 6.87\%$. b) Refined neutron diffraction pattern with agreement factors of $R_{wp} = 6.40\%$, $R_p = 4.95\%$, $R_F^2 = 6.83\%$. For each pattern, the collected data are in red, the fit is shown in black, the calculated reflections of Li_2FePO_4F are shown in blue, calculated reflections of Al are shown in green and the difference map is shown in grey. A summary of the refined data is given in Table 2 and a summary of Fe co-ordination environments is given in Table 3.

Table 2 Lattice constants and atomic parameters of Li_2FePO_4F determined by a combined refinement of X-ray and neutron powder diffraction data. Agreement factors for neutron diffractrion data: $R_{wp} = 6.40\%$, $R_p = 4.95\%$, $R_F^2 = 6.83\%$ Agreement factors for X-ray diffraction data: $R_{wp} = 9.48\%$, $R_p = 7.32\%$, $R_F^2 = 6.87\%$ Agreement factors for combined refinement: $R_{wp} = 9.45\%$, $R_p = 7.29\%$, $\chi^2 = 45.79$

Li_2FePO_4F

Space group: $P\bar{1}$ (#2), Triclinic
$M_w = 183.70$ g mol^{-1}
$D = 3.225$ g cm^{-3}
$a = 5.3736(2)$ Å
$b = 7.4791(2)$ Å
$c = 5.3276(2)$ Å
$\alpha = 108.398(4)°$
$\beta = 94.615(4)°$
$\gamma = 108.217(4)°$
$V = 189.142(8)$ Å^3

Atom	Wych.	x/a	y/b	z/c	Occ.	U_{iso}
Fe (1)	1*a*	0	0	0	1.0	0.011(2)
Fe (2)	1*b*	0	1/2	0	1.0	0.008(1)
P	2*i*	0.6389(9)	0.750(1)	0.348(1)	1.0	0.011(1)
O (1)	2*i*	0.657(2)	0.866(2)	0.147(2)	1.0	0.015(3)
O (2)	2*i*	0.335(2)	0.635(1)	0.309(2)	1.0	0.018(3)
O (3)	2*i*	0.790(2)	0.620(2)	0.304(2)	1.0	0.012(3)
O (4)	2*i*	0.278(2)	0.097(2)	0.365(2)	1.0	0.017(3)
F	2*i*	0.888(1)	0.262(2)	0.171(2)	1.0	0.013(2)
Li (1)	2*i*	0.465(5)	0.679(4)	0.743(5)	1.0	0.015
Li (2)	1*g*	0	1/2	1/2	1.0	0.015
Li (3)	2*i*	0.112(5)	0.824(7)	0.521(8)	0.5	0.015

Table 3 Summary of Bond Distances for Each Iron Environment in Li_2FePO_4F

Atom	Ligand	Multiplicity	Distance (Å)
Fe1	O2	2×	2.0739
	O3	2×	2.1372
	F1	2×	2.1919
	Li2	2×	2.6638
Fe2A	O4	2×	2.1251
	O1	2×	2.1408
	F1	2×	2.1718
	Li3	2×	2.6872
Fe2B	O4	2×	2.1251
	O1	2×	2.1408
	F1	2×	2.1718

crystallographically unique Li sites were identified in Li_2FePO_4F. A graphical representation of the structure is shown in Fig. 11a. Li1 is positioned close to the centroid of the split Li position in the parent $LiFePO_4F$. The new environment for this Li ion is smaller than that in $LiFePO_4F$, owing to the significantly larger size of the Fe^{2+} ion (78 pm radius, compared to Fe^{3+} with a radius of 64 pm)[34] which forces atoms closer to Li1. As a consequence, the new Li position is not split. The two sites where the intercalated Li reside are Li2 and Li3, each of which is occupied by 0.5 Li. Li2 resides between the chains of Fe octahedra on a special position, the 1g site and is coordinated by two fluorine and four oxygen ligands. A previous study of a natural (slightly reduced) sample of $LiFePO_4(OH)$ showed this site is partially occupied by Fe^{2+} ions.[35] The electrochemical and powder XRD data (*vide supra*) suggest that occupation of this site does not induce a two-phase transition until full insertion is achieved at $x = 0.5$. The Li3 site is a general position which is half occupied and octahedrally coordinated by one fluorine and five oxygen ligands.

With the intercalated Li ions occupying these two sites, the Mössbauer results can be put into structural context. Fig. 11b is a graphical representation of the bonding environment of the Fe1 ion. The Fe–O and Fe–F bond distances range from 2.07 to 2.19 Å (see Table 3). Li2 resides between adjacent chains of Fe octahedra and each Fe1 shares triangular faces with two Li2 ions which are 2.66 Å from Fe1. These Li^+ ions are close enough to the

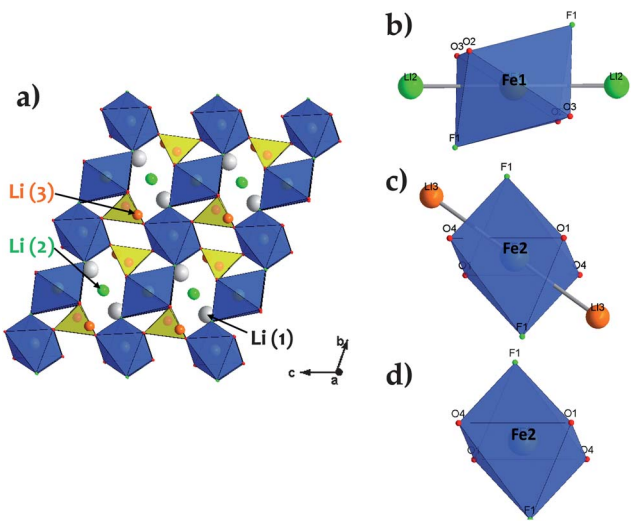

Fig. 11 a) Graphical representation of the structure of Li_2FePO_4F with iron environments Fe1, Fe2A and Fe2B highlighted (b, c, d respectively). Phosphate tetrahedra are depicted in yellow, iron octahedra in blue, Li1 in white, Li2 in green and Li3 in orange.

Fe1 site that the Li can be considered part of the Fe bonding environment. Representations of the Fe2 site are shown in Fig. 11c–d. The Fe–O and Fe–F bonds range from 2.12 to 2.17 Å in length and the Li3 ion is also in close proximity to Fe2 (2.68 Å). If the Li3 site were fully occupied, each Fe2 ion would be face-shared with two Li octahedra, just as the case of the Fe1 site. As the Li3 site is only half occupied, only half of the Fe ions on the Fe2 site will face-share with two Li3 ions (denoted as the Fe2A site, see Fig. 11c). The remaining Fe2 sites (denoted as Fe2B sites, Fig. 11d) will not have any cations in the local environment. The similar environments of the Fe1 and Fe2A atoms can not be resolved by Mössbauer spectroscopy and therefore, the ratio of [Fe1 + Fe2A] sites to the Fe2B sites in Li_2FePO_4F is 3 : 1, which is in accord with the Mössbauer data. Finally, we note that the tavorite-type structure of Li_2FePO_4F prepared by reduction of $LiFePO_4F$ differs greatly from Li_2FePO_4F prepared by ion-exchange of two-dimensional Na_2FePO_4F.[36]

Conclusions

Simple and environmentally friendly hydro- and solvothermal methods provide easy routes to the synthesis of $LiFePO_4F_{1-x}(OH)_x$, although careful manipulation of the pH, precursors and solvent are necessary to produce pure tavorite-type phases. The higher electronegativity of F^- compared to OH^- serves to increase the thermal stability of $LiFePO_4F$ compared to $LiFePO_4(OH)$, and also raise the electrode potential from 2.40 V for $LiFePO_4(OH)$, to 2.75 V for $LiFePO_4F$, as a consequence of the enhanced inductive effect. Both $LiFePO_4(OH)$ and $LiFePO_4F$ demonstrate two-phase behavior in Li cells, although particle size has a significant effect on the capacity and in the case of $LiFePO_4(OH)$, the potential itself. The two-phase nature of $LiFePO_4F$ intercalation was confirmed by chemical reduction of $LiFePO_4F$ where $Li_{1+x}FePO_4F$ compositions clearly show a mixture of $LiFePO_4F$ and Li_2FePO_4F. The refined structure of Li_2FePO_4F shows that the corner-shared framework of the "$FePO_4F$" lattice remains intact upon reduction to Li_2FePO_4F. Lithium insertion in the lattice is complex, and two sites are occupied. Occupation of the first appears to occur *via* a solid solution process (with respect to lithium concentration), whereas occupation of the last site triggers two-phase behavior. The overall 8.0% volume expansion of the lattice upon insertion of one Li is a likely origin of the two-phase nature of this compound.

Acknowledgements

LFN and DHR acknowledge the generous financial support of the NSERC through its Discovery, and Collaborative Research Development programs. Additional support was provided by NSERC through a Canada Research Chair (to LFN) and by FQRNT (Fonds Québecois de la Recherche sur la Nature et les Technologies, to DHR). We thank the Oakridge National Laboratory for providing neutron beam time, and we are especially grateful to Dr. Ovidiu Garlea at ORNL for his acquisition of the powder neutron diffraction data.

References

1 A. K. Pahdi, K. S. Nanjundaswamy and J. B. Goodenough, *J. Electrochem. Soc.*, 1997, **144**, 1188–1194.
2 A. K. Pahdi, K. S. Nanjundaswamy, C. Masquelier, S. Okada and J. B. Goodenough, *J. Electrochem. Soc.*, 1997, **144**, 1609–1613.
3 J. Li, W. Yao, S. Martin and D. Vaknin, *Sol. Stat. Ion*, 2008, **179**, 2016–2019.
4 M. Gaberscek, R. Dominko and J. Jamnik, *Electrochem. Commun.*, 2007, **9**, 2778–2873.
5 H. Huang, S. C. Yin and L. F. Nazar, *Electrochem. Solid-State Lett.*, 2001, **4**, A170–A172.
6 P. S. Herle, B. Ellis, N. Coombs and L. F. Nazar, *Nat. Mater.*, 2004, **3**, 147–152.
7 B. L. Ellis, W. R. M. Makahnouk, W. N. Rowan-Weetaluktuk, D. H. Ryan and L. F. Nazar, *Chem. Mater.*, 2010, **22**, 1059–1070.
8 N. Recham, J.-N. Chotard, L. Dupont, K. Djellab, M. Armand and J.-M. Tarascon, *J. Electrochem. Soc.*, 2009, **156**, A993–A999.
9 T. N. Ramesh, K. T. Lee, B. L. Ellis and L. F. Nazar, *Electrochem. Solid-State Lett.*, 2010, **13**, A43–A47.
10 N. Recham, J.-N. Chotard, J.-C. Jumas, L. Laffont, M. Armand and J.-M. Tarascon, *Chem. Mater.*, 2010, **22**, 1142–1148.
11 J. Barker, M. Y. Saidi and J. L. Swoyer, *J. Electrochem. Soc.*, 2003, **150**, A1394–A1398.
12 J. Barker, R. K. B. Gover, P. Burns, A. Bryan, M. Y. Saidi and J. L. Swoyer, *J. Power Sources*, 2005, **146**, 516–520.
13 R. Tripathi, T. N. Ramesh, B. L. Ellis and L. F. Nazar, *Angew. Chem., Int. Ed.*, 2010, **49**, 8738–8742.
14 N. Recham, J.-N. Chotard, L. Dupont, C. Delacourt, W. Walker, M. Armand and J.-M. Tarascon, *Nat. Mater.*, 2010, **9**, 68–74.
15 M. S. Whittingham, Y. Song, S. Lutta, P. Y. Zavalij and N. A. Chernova, *J. Mater. Chem.*, 2005, **15**, 3362–3379.
16 L. Sebastian and J. Gopalakrishnan, *J. Mater. Chem.*, 2003, **13**, 433–441.
17 L. Sebastian, J. Gopalakrishnan and Y. Piffard, *J. Mater. Chem.*, 2002, **12**, 374–377.
18 S. Yang, P. Y. Zavalij and M. S. Whittingham, *Electrochem. Commun.*, 2001, **3**, 505–508.
19 B. Ellis, W. H. Kan, W. R. M. Makahnouk and L. F. Nazar, *J. Mater. Chem.*, 2007, **17**, 3248–3254.
20 J. Barker, M. Y. Saidi and J. L. Swoyer, *J. Electrochem. Soc.*, 2004, **151**, A1670–A1677.
21 N. Marx, L. Croguennec, D. Carlier, A. Wattiaux, F. Le Cras, E. Suard and C. Delmas, *Dalton Trans.*, 2010, **39**, 5108–5116.
22 P. Barpanda, J.-N. Chotard, N. Recham, C. Delacourt, M. Ati, L. Dupont, M. Armand and J.-M. Tarascon, *Inorg. Chem.*, 2010, **49**, 7401–7413.
23 J. Barker, R. K. B. Gover, P. Burns and A. Bryan, *Electrochem. Solid-State Lett.*, 2005, **8**, A285–A287.
24 P. P. Prosini, M. Carewska, S. Scaccia, P. Wisniewski, S. Passerini and M. Pasquali, *J. Electrochem. Soc.*, 2002, **149**, A886–A890.
25 A. C. Larson and R. B. Von Dreele, *Los Alamos National Laboratory Report LAUR 86-748*, 2000.
26 B. H. Toby, *J. Appl. Crystallogr.*, 2001, **34**, 210–213.
27 T. Roncal-Herrero, J. D. Rodriguez-Blanco, L. G. Benning and E. H. Oelkers, *Cryst. Growth Des.*, 2009, **9**, 5197–5205.
28 J. L. Pizzaro-Sanz, J. M. Dance, G. Villeneuve and M. I. Arriortua-Marcaida, *Mater. Lett.*, 1994, **18**, 327–330.
29 S. Yang, P. Y. Zavalij and M. S. Whittingham, *Electrochem. Commun.*, 2001, **3**, 505–508.
30 L. Domange, *Ann. Chim.*, 1937, **7**, 235–297.
31 N. Meethong, H.-Y. S. Huang, W. C. Carter and Y.-M. Chiang, *Electrochem. Solid-State Lett.*, 2007, **10**, A134–A138.
32 K. T. Lee, W. H. Kan and L. F. Nazar, *J. Am. Chem. Soc.*, 2009, **131**, 6044–6045.
33 R. Dominko, *J. Power Sources*, 2008, **184**, 462–468.
34 R. D. Shannon, *Acta Crystallogr., Sect. A: Cryst. Phys., Diffr., Theor. Gen. Crystallogr.*, 1976, **A32**, 751–767.
35 O. V. Yakubovich and V. S. Urusov, *Geokhimiya*, 1997, **7**, 720–729.
36 B. Ellis, W. R. M. Makahnouk, Y. Makimura, K. Toghill and L. F. Nazar, *Nat. Mater.*, 2007, **6**, 749–753.